5

COMPARISON OF CONVERGENCE RATES OF THE CONJUGATE GRADIENT METHOD APPLIED TO VARIOUS INTEGRAL EQUATION FORMULATIONS

D. R. Wilton, and J. E. Wheeler III

5.1 Introduction

It is well known that the scattering properties of conducting objects at frequencies up through the first few scatterer resonances may be effectively and accurately computed by numerically solving an integral equation for the induced surface current density via the method of moments. At higher frequencies, however, the computational burden of this approach can become excessive. For example, the surface area of a three-dimensional object with some characteristic dimension of length m in wavelengths—and hence the number of unknown currents in a subdomain basis representation—is of order m^2. The corresponding moment matrix is of order $m^2 \times m^2$, and hence the memory storage and time required to fill the matrix are of order m^4. For large matrices of order $N \times N$, the time required to solve the associated matrix equation is dominated by the approximately $N^3/3$ multiplications required in the Gaussian elimination process; hence for a moment

matrix of order $m^2 \times m^2$, this implies a solution time of order m^6. The solution time increases still further if the moment matrix becomes so large that most of the elements must be stored on a mass storage device with a much slower access time. The additional time required to fetch such elements can easily become the dominant factor in the overall solution time. These considerations merely point to the fact that a three-dimensional object of seemingly modest electrical dimensions may in fact require enormous computer resources in time and memory for the prediction of the object's electromagnetic scattering characteristics.

In order to retain many of the advantages of the integral equation and moment method formulations while reducing the computer resources required, a number of authors [1–5] have investigated the use of the conjugate gradient method (CGM) as an alternative to Gaussian elimination in the linear equation solving step of the solution process. Since CGM is an iterative procedure, it can reduce the total solution time if the process converges in only a few iterations. Even if a relatively large number of iterations are required, the approach may also save time by obviating the need for mass storage. Since in each iteration step the matrix elements may be used as they are computed, it is not necessary to store matrix elements out of core if it is feasible to recompute them as needed during the course of the computation. In many cases, it is faster to recompute needed elements than to access them from a mass storage device.

Much of current research in the use of CGM is concerned with various approaches to pre-conditioning the moment matrix to accelerate convergence of the method [6,7]. In this section we show that poor conditioning of the matrix is often linked to the problem formulation, however, and that significant improvement in the conditioning can be obtained by utilizing an alternate formulation of the problem. We compare, for example, the electric field (EFIE), magnetic field (MFIE), and combined field (CFIE) integral equation formulations for scattering by a two dimensional circular cylinder. We also apply the CGM to the three-dimensional problems of a sphere and finite circular cylinder, both excited by a voltage source. Since the CFIE is not easily applied to antenna radiation problems, the so-called combined source integral equation (CSIE) is used for these problems.

In the following section, the various integral equation formulations and the uniqueness properties of their solutions are briefly reviewed.

The conjugate gradient method is also summarized in Section 5.3, and numerical results for the different formulations at a number of representative frequencies and for the different geometries are presented in Section 5.4.

5.2 Integral Equation Formulations

Electric field integral equations are frequently used because they apply to both open and closed bodies. For open bodies, the equivalent surface current found as a solution to the equation is actually the vector sum of the currents on opposite sides of the surface. The EFIE follows from enforcing the condition that the tangential electric field (sum of the incident field $\mathbf{E}^i$ and the scattered field $\mathbf{E}^s$) vanish on the body surface S:

$$\hat{\mathbf{n}} \times \mathbf{E}^i + \hat{\mathbf{n}} \times \mathbf{E}^s = 0, \quad \mathbf{r} \in S \tag{1}$$

where $\mathbf{E}^s$ is expressed in terms of the magnetic vector potential $\mathbf{A}$ and the scalar electric potential Φ as

$$\mathbf{E}^s = -j\omega\mathbf{A} - \nabla\Phi \tag{2}$$

For a two-dimensional cylinder in which the illumination is assumed invariant along the cylinder axis, it is sufficient to enforce the boundary condition at each point ρ on C, the cylinder cross section (Fig. 5.1): For illumination perpendicular to and polarized transverse magnetic (TM) to the cylinder axis, only z-components of electric field and surface current are present, and expressing the scattered electric field in (1) in terms of potential integrals yields

$$jk\eta \int_C J_z(\rho')G(\rho, \rho')d\ell' = E_z^i(\rho), \quad \rho \in C \tag{3}$$

where J_z is the unknown axial component of the surface current density on the cylinder. For the corresponding transverse electric (TE) case, only the transverse component of electric field is present and (1) becomes

$$\begin{aligned} j\frac{\eta}{k}\Big\{k^2 \int_C J_\ell(\rho')\hat{\ell} \cdot \hat{\ell}' G(\rho, \rho')d\ell' + \\ \frac{d}{d\ell}\int_C \frac{dJ_\ell(\rho')}{d\ell'} G(\rho, \rho')d\ell'\Big\} = E_\ell^i(\rho), \quad \rho \in C \end{aligned} \tag{4}$$

where

$$G(\rho, \rho') = \frac{1}{4j} H_0^{(2)}(k|\rho - \rho'|) \tag{5}$$

and $H_0^{(2)}$ is the Hankel function of the second kind and zero order. For closed bodies, Eqs. (3) and (4) apply for excitations whose axially independent sources are located either interior or exterior to the cylinder. But at frequencies for which the two-dimensional conducting cavity with cross section C is resonant (or equivalently, at frequencies for which the waveguide with cross section C is cutoff), the associated cavity modal wall currents automatically satisfy the boundary conditions implied by (3) or (4) with no excitation present. That is, at such frequencies, a homogeneous solution of (3) or (4) exists, implying that the corresponding moment matrix is singular and hence that a unique solution to the scattering problem does not exist. In practice, the moment matrices are usually only nearly singular, but the numerically obtained surface currents are contaminated by the homogeneous solution near such a resonant frequency [8]. It is noted that the singular frequencies of (3) and (4) coincide with the waveguide cutoff frequencies of the TM and TE waveguide modes, respectively, and for a cylinder of arbitrary cross section are not generally known *a priori*.

The magnetic field integral equation [9] may be obtained by requiring the total tangential magnetic field (the sum of the incident field $\mathbf{H}^i$ and the scattered field $\mathbf{H}^s$) to vanish just *inside* the surface the conductor; that is we require

$$\hat{\mathbf{n}} \times \mathbf{H}^i + \hat{\mathbf{n}} \times \mathbf{H}^s = 0, \qquad \mathbf{r} \uparrow S \tag{6}$$

where '$\mathbf{r} \uparrow S$' indicates that the observation point $\mathbf{r}$ approaches S from the interior. The scattered magnetic field is, in turn, expressed in terms of the magnetic vector potential as

$$\mathbf{H}^s = \frac{1}{\mu} \nabla \times \mathbf{A} \tag{7}$$

For a cylinder under TM illumination, a careful analysis of the limit results in the integral equation

$$\frac{J_z(\rho)}{2} - \frac{k}{4j} \int_C J_z(\rho') \cos\theta H_1^{(2)}(k|\rho - \rho'|) d\ell' = H_z^i(\rho), \quad \rho \in C \tag{8}$$

where

$$\cos\theta = \hat{\mathbf{n}} \cdot \frac{(\boldsymbol{\rho} - \boldsymbol{\rho}')}{|\boldsymbol{\rho} - \boldsymbol{\rho}'|} \tag{9}$$

and under TE illumination to

$$\frac{J_\ell(\boldsymbol{\rho})}{2} - \frac{k}{4j}\int_C J_\ell(\boldsymbol{\rho}')\cos\theta' H_1^{(2)}(k|\boldsymbol{\rho} - \boldsymbol{\rho}'|)d\ell' = -H_z^i(\boldsymbol{\rho}), \quad \boldsymbol{\rho} \in C \tag{10}$$

where

$$\cos\theta' = \hat{\mathbf{n}}' \cdot \frac{(\boldsymbol{\rho} - \boldsymbol{\rho}')}{|\boldsymbol{\rho} - \boldsymbol{\rho}'|} \tag{11}$$

The MFIE formulation also has homogeneous solutions (and hence is singular) at certain specific frequencies. The boundary condition implied by (6) permits us to identify these as the resonant frequencies of a cavity with *magnetic* walls. Using electromagnetic duality [10] to interchange the roles of electric and magnetic fields, however, we see that (6) is mathematically equivalent to (1). The field quantities in (1) and (6) implicitly satisfy the Helmholtz wave equation interior to S and explicitly satisfy equivalent boundary conditions on S; hence the formulations represented by these equations have the same singular frequencies [8]. In two-dimensions, however, the roles of the axial electric and magnetic fields are reversed by the duality argument, and the singular frequencies of the TM form of the MFIE (8) are thus found to be identical with the TE resonances of the conducting cylinder formed by C. Similarly, the singular frequencies of the TE form of the MFIE (10) correspond to the TM cylinder resonances. Hence the singular frequencies of (3) and (10) are identical, as are those of (4) and (8).

The above duality argument applies *only* to the boundary conditions from which the MFIE is derived. In treating the sources in (8) and (10) by the duality argument, one must also replace the unknown electric current by its dual, a *magnetic* current. Thus, although the integral equations have the same singular frequencies, the homogeneous solutions of (3) represent *electric* current sources which support the TM cavity modes interior to C, while those of the dual to (10) represent equivalent *magnetic* currents supporting these modes. Similarly, the homogeneous solutions of (4) represent electric current sources which support the TE cavity modes in C, while those of the dual to (8) represent equivalent magnetic currents which support these modes.

By the above argument, (3) and (6) generally have different singular frequencies, and hence it is perhaps not surprising that a linear

combination of the two integral equations can have a unique solution at the singular frequencies of one of the original equations. Similarly, a linear combination of (4) and (10) can have the same property. In three-dimensions, however, the EFIE and the MFIE do not generally decompose into different polarizations with different resonant frequencies. Hence, it is at first surprising that, as proved by Mautz and Harrington [8], certain linear combinations of the two formulations have no singular frequencies. That a linear combination of the two singular linear operators is non-singular is due to the fact that the *homogenous solutions of the two operators are different*; one represents the *electric* currents which support the electric wall cavity modes, while the other can be thought of as the dual of the equivalent *magnetic* currents which support electric wall cavity modes. The resulting formulation obtained by taking a linear combination of the two formulations is called the combined field integral equation (CFIE) [8] and is written in the following form:

$$-\hat{\mathbf{n}} \times \mathbf{H}^s(\mathbf{r}) - \frac{\alpha}{\eta}\mathbf{E}^s_{tan}(\mathbf{r}) = \hat{\mathbf{n}} \times \mathbf{H}^i(\mathbf{r}) + \frac{\alpha}{\eta}\mathbf{E}^i_{tan}(\mathbf{r}), \quad \mathbf{r} \uparrow S \tag{12}$$

in which α is a positive real number, generally taken to be unity. The intrinsic impedance factor, η, merely insures that the contributions from each equation are given approximately equal weight when α is set equal to unity. It is shown in [8] that this linear combination eliminates the singularities in the operators that are present in both the EFIE and MFIE formulations. Although not mentioned in [8], it is easily shown that, in contrast to the MFIE, the CFIE can be used to analyze both open and closed structures; unlike the EFIE, however, it must be used to determine the currents flowing on *both* sides of an open surface. Thus for open surfaces and for the same surface discretization, the CFIE requires twice as many unknowns to be determined as does the EFIE alone.

A significant disadvantage of the CFIE becomes apparent when one attempts to excite a structure with a voltage source. In this case the incident magnetic field is unknown and the CFIE is not useful. An alternative formulation which retains the conditioning properties of the CFIE while requiring knowledge of only the incident electric field was noted by Mautz and Harrington [11]. This formulation, the combined source integral equation (CSIE), introduces a magnetic current defined in terms of the electric current sources as

$$\mathbf{M} = \alpha\eta\hat{\mathbf{n}} \times \mathbf{J} \tag{13}$$

in which α is again a positive constant, taken as unity in our comparisons. The new set of equivalent currents must be chosen such that they produce the correct fields exterior to the body. However, the introduction of the magnetic current also causes a jump in the tangential surface electric field so that the fields interior to the body are not zero as in the previous integral equations considered. Since the electric current must support the discontinuity in the tangential magnetic field, which is no longer zero in the interior, the electric current is not the physical electric current, but only an equivalent current. The integral equation still follows from (1), but now the scattered electric field is generated by the combined electric and magnetic sources and is expressed in terms of potentials as

$$\mathbf{E}^s = -j\omega\mathbf{A} - \nabla\Phi - \frac{1}{\epsilon}\nabla \times \mathbf{F} \tag{14}$$

where $\mathbf{F}$ is the electric vector potential [10] due to the dependent magnetic current. Mautz and Harrington [11] show that the resulting operator is identical to the transpose of the CFIE operator with the basis and testing functions interchanged. In the examples, the CSIE is applied to the three-dimensional problems of a sphere and finite circular cylinder, and their convergence properties under the conjugate gradient solution method are compared with those resulting from the corresponding EFIE formulation.

5.3 Overview of the Conjugate Gradient Method

CGM is an iterative solution method in which a quadratic functional is minimized along successive vectors in a manner similar to the steepest descent method. In contrast to the steepest descent method, however, the direction vectors are chosen to satisfy a so-called mutual conjugate property, and, for an $N \times N$ linear system, the method yields the exact solution in no more than N steps *in the absence of roundoff error.* An adequate solution may often be obtained in fewer than N steps. In poorly conditioned problems, however, the algorithm may converge slowly or, due to accumulation of roundoff error, not at all.

While Gaussian elimination requires approximately $N^3/3$ multiplications for N large, an M-step CGM solution requires approximately $2MN^2$ multiplications. Therefore, assuming the entire matrix

can be stored in a computer's random access memory, CGM is not competitive with Gaussian elimination in terms of computation time unless M is less than about $N/6$. If at least part of the matrix must be stored in mass memory, however, CGM with matrix element regeneration may still be faster than Gaussian elimination. For illustrative purposes the CGM algorithm given in [12] is listed below. The matrix A^* used below is the complex conjugate transpose of A.

To solve the system $A\mathbf{x} = \mathbf{h}$, given an initial guess $\mathbf{x}_0$ and normalized residual tolerance ϵ, the following procedure is performed.

- Compute the initial residual and direction vectors:

$$\mathbf{r}_0 = \mathbf{h} - A\mathbf{x}_0, \quad \mathbf{p}_0 = A^*\mathbf{r}_0$$

- Perform the iterative procedure:

For $i = 0$ to $N - 1$

1. $a_i = \frac{||A^*\mathbf{r}_i||^2}{||A\mathbf{p}_i||^2}$
2. $\mathbf{x}_{i+1} = \mathbf{x}_i + a_i\mathbf{p}_i$
3. $\mathbf{r}_{i+1} = \mathbf{r}_i - a_iA\mathbf{p}_i$
4. If the *normalized residual* $\frac{||\mathbf{r}_{i+1}||}{||\mathbf{h}||} \leq \epsilon$, then exit
5. $b_i = \frac{||A^*\mathbf{r}_{i+1}||^2}{||A^*\mathbf{r}_i||^2}$
6. $\mathbf{p}_{i+1} = A^*\mathbf{r}_{i+1} + b_i\mathbf{p}_i$
7. Next i

It should be noted that the algorithm actually solves the system $A^*A\mathbf{x} = A^*\mathbf{h}$, which has the same solution as $A\mathbf{x} = \mathbf{h}$ but for which the operator A^*A is positive definite and Hermitian. Each step requires only the computation of matrix and vector inner products involving A or its complex conjugate transpose. Since the residual is available at each step, it can be used to estimate a bound on the relative solution error as [13]

$$\frac{||\mathbf{x} - \mathbf{x}_{i+1}||}{||\mathbf{x}||} \leq \kappa \frac{||A^*\mathbf{r}_{i+1}||}{||A^*\mathbf{h}||} \tag{15}$$

where κ is the *condition number* of A^*A, the product of the norm of A^*A and that of its inverse using any valid norm. In the L_2 norm, κ is called the *spectral condition number* and is given by

$$\kappa = \frac{\lambda_{max}}{\lambda_{min}} \tag{16}$$

where λ_{max} and λ_{min} are the maximum and minimum eigenvalues of the positive definite Hermitian matrix A^*A. The order of magnitude of the condition number may be taken as a rough measure of the number of significant digits that may be lost in the solution during the course of its computation, and hence it is near unity in a well-conditioned system and is large in a poorly conditioned system. As (15) shows, one cannot guarantee an accurate solution in the i-th iteration even if the norm of the residual is small unless the condition number is reasonably small. If roundoff error is significant, the method may converge slowly or not at all. We further note that if neither $\mathbf{p}_i$ nor $\mathbf{r}_{i+1}$ is zero, but either $A\mathbf{p}_i$ or $A^*\mathbf{r}_{i+1}$ vanishes, then the iteration procedure stagnates. These conditions can occur, of course, only if A has homogeneous solutions, i.e., if A is singular.

5.4 Numerical Results

Since our interest in CGM is as an alternative to solving large matrices associated with high frequency scattering, it is appropriate to review our observations concerning the solution of scattering problems at high frequencies:

- At frequencies near interior resonances of a closed scatterer, the system matrix becomes ill-conditioned for both the EFIE and the MFIE formulations. It is difficult to insure avoidance of these frequencies since they cannot, in general, be determined *a priori*. Furthermore, the deficiency is more serious at high frequencies since the spectral density of the resonances increases with frequency. Use of the CFIE or CSIE, on the other hand, eliminates this difficulty.
- Near an interior resonant frequency, an eigenvalue of the EFIE or MFIE system matrix approaches zero. Thus, by (16), the condition number becomes large, and, in the presence of roundoff error, (15) implies that convergence is difficult to achieve.

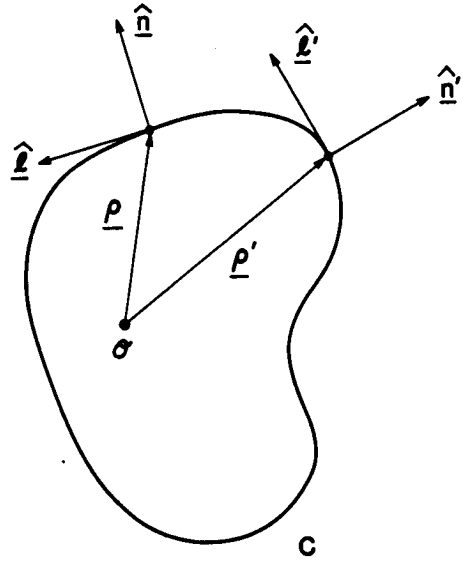

Figure 5.1 Cross section of perfectly conducting cylinder.

The above statements suggest that use of the CFIE or CSIE not only would eliminate the difficulties associated with non-uniqueness of solutions of integral equations at high frequencies, but would also enhance the convergence properties of the CGM since the small eigenvalues near interior resonant frequencies are eliminated. In this section, examples are presented to illustrate this idea for at least the limited class of problems considered here.

We investigate the problem of scattering by a circular cylinder illuminated by TE and TM incident waves. Illustrated in Fig. 5.2 is the spectral condition number associated with the moment matrices of the EFIE, MFIE, and CFIE formulations for the TM polarization. For this calculation, the cylinder was subdivided into 200 segments at all frequencies considered. Similar information is presented in Fig. 5.3 for the TE polarization. The cavity resonances are clearly evident in both figures as singularities in the condition number. Note that in Fig. 5.2, the peaks are observed in the EFIE solution at the resonant frequencies of the TM circular waveguide modes while those of the MFIE solution are seen to be at the resonant frequencies of the TE waveguide modes; this correspondence is reversed for the TE polarization, as depicted in Fig. 5.3. One easily verifies that these frequencies are indeed those for which

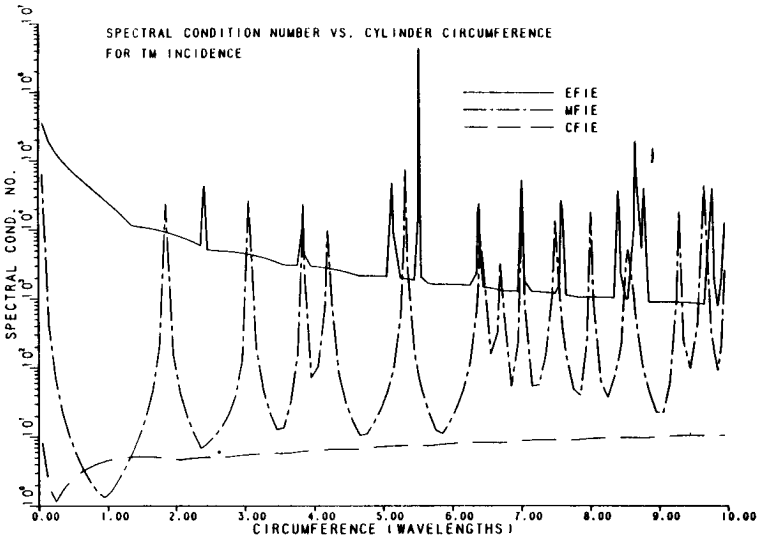

Figure 5.2 Spectral condition number vs. circumference for a circular cylinder illuminated by a TM plane wave. Cylinder geometry approximated by 200 straight line segments.

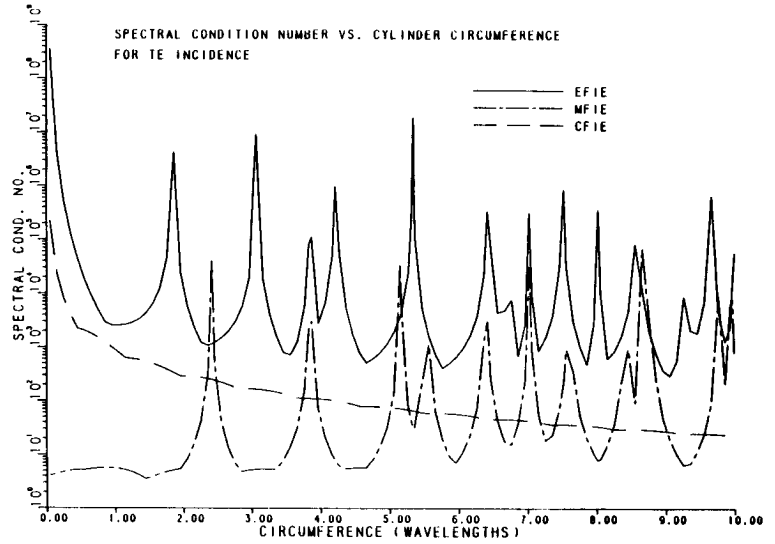

Figure 5.3 Spectral condition number vs. circumference for a circular cylinder illuminated by a TE plane wave. Cylinder geometry approximated by 200 straight line segments.

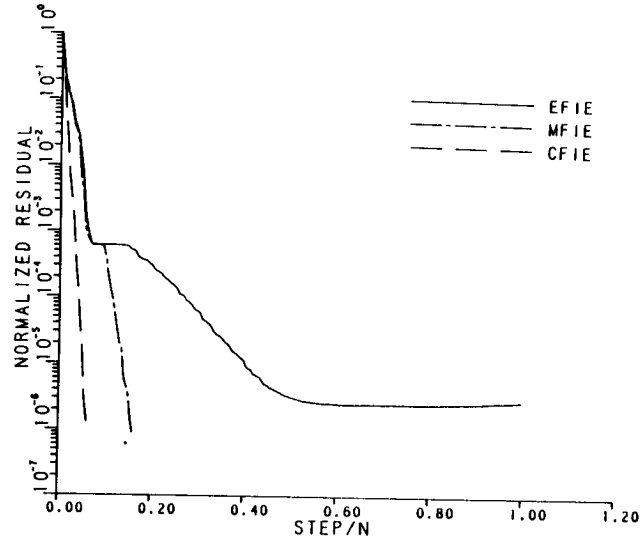

Figure 5.4 Normalized residual vs. normalized iteration number for TM case at a resonant frequency ($ka = 10.173$). Computations performed using 32 bit (7-8 significant figure) word lengths and 200 unknowns.

$$J_n(ka) = 0 \tag{17}$$

for the TM modes and

$$J_n'(ka) = 0 \tag{18}$$

for the TE modes, where $J_n(x)$ and $J_n'(x)$ are the Bessel function and its first derivative, respectively. The figures also clearly illustrate the increasing spectral density of the resonances with increasing frequency. One observes that the EFIE formulation generally results in a more poorly conditioned system of equations than the MFIE formulation. The condition number of the CFIE, on the other hand, is practically monotonic in frequency, and remains near unity at high frequencies.

The effects of cavity resonances on the CGM convergence rates of the three formulations are illustrated by comparing these rates both at resonant and non-resonant frequencies of the circular cylinder. A 200×200 matrix is solved in each case on a DEC MicroVAX II computer, and round-off error effects and their dependence on conditioning are deduced by solving the systems using both 32 (single precision) and 64 bit (double precision) word length computer arithmetic.

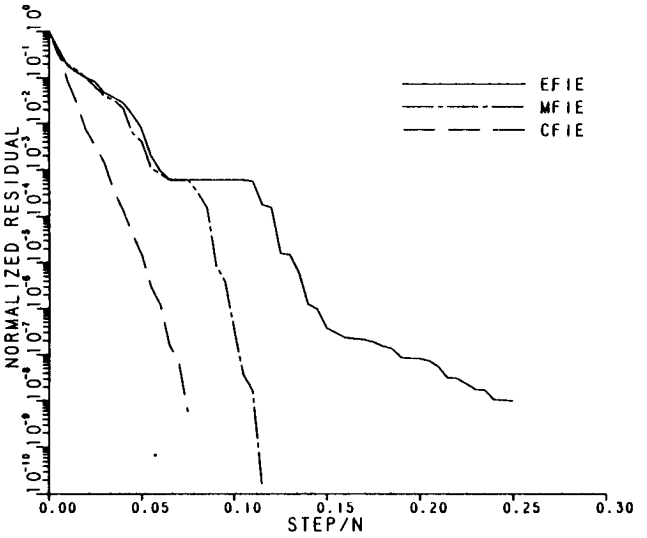

Figure 5.5 Normalized residual vs. normalized iteration number for TM case at a resonant frequency ($ka = 10.173$). Computations performed using 64 bit (16–17 significant figure) word lengths and 200 unknowns.

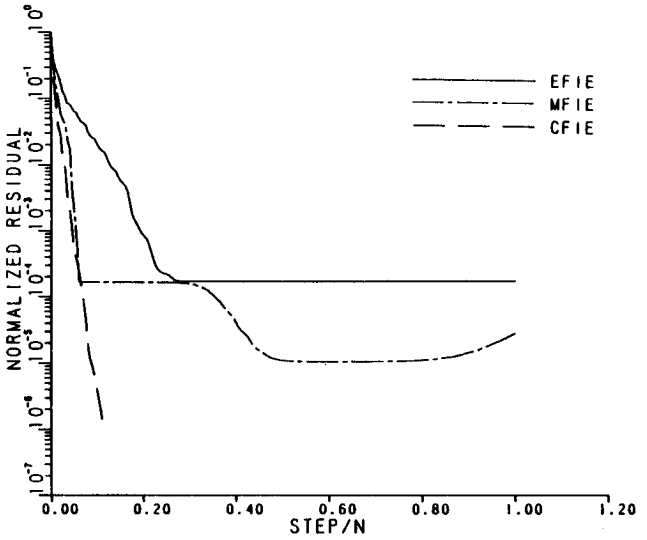

Figure 5.6 Normalized residual vs. normalized iteration number for TE case at a resonant frequency ($ka = 10.173$). Computations performed using 32 bit (7–8 significant figure) word lengths and 200 unknowns.

Figure 5.4 illustrates the convergence rate of the normalized residual of the CGM algorithm for the TM polarization at the circular cylinder resonant frequency $ka = 10.173$. This resonance is a convenient choice because it is a resonant frequency for both the TE and TM polarizations. The horizontal axis represents the iteration step number normalized to the theoretical maximum number of steps, N. Note that both the EFIE and MFIE residuals reach 'plateaus' in which, for several iterations, no further reduction in the residual is achieved. In fact, once the residual reaches a level of about 10^{-6}, the residual actually increases slightly after each step due to the accumulation of roundoff error.

To confirm the effect of roundoff error, the calculations were repeated in double precision with the results appearing in Fig. 5.5. The early iterations yield approximately the same residual*, and also tend to reach a plateau, as in Fig. 5.4, but the EFIE solution is able to converge to a much smaller residual (note the different scales in the figures). On the other hand, the convergence of the CFIE, whose condition number is insensitive to resonant frequency, is much faster than that of either the EFIE or the MFIE. The rate is also monotonic. Because the associated matrix is well-conditioned, there is essentially no change in the convergence rate when double precision is used. An important observation is that convergence is achieved in *significantly fewer than N/6 steps*, the approximate maximum number for which CGM is faster than Gaussian elimination in core for large N and a single right hand side.

These same effects are illustrated even more dramatically in Figs. 5.6 and 5.7, which show the corresponding results for the TE polarization. In this case a plateau occurs when the residual reaches about 10^{-4} for both the EFIE and MFIE. The residual of the EFIE is not reduced with further iterations in the single precision case (Fig. 5.6), and is reduced further only after many steps in the double precision case (Fig. 5.7). The CFIE, on the other hand, converges relatively quickly and is essentially unaffected by the increase in precision. An unexplained observation in Figs. 5.4–5.7 is the fact that even though different formulations are used, the plateaus of the residuals appear to have identical levels for the EFIE and MFIE cases; the levels of the plateaus also change in going from single to double precision.

---

* Actually a small improvement in the convergence rate is obtained, presumably due to the reduced effects of error accumulation.

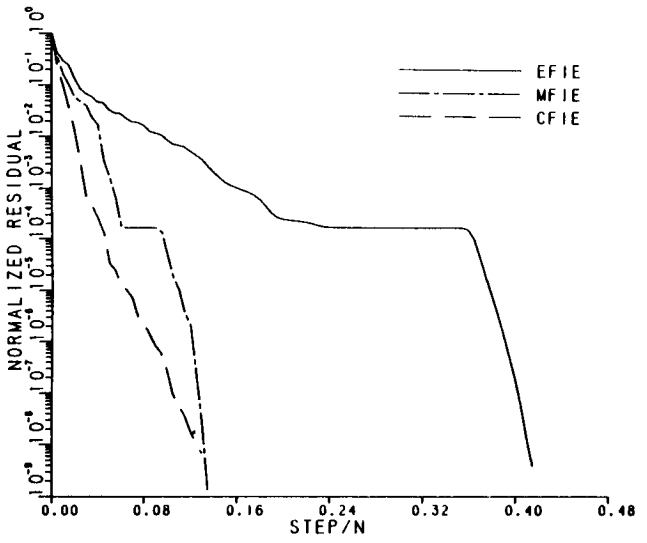

Figure 5.7 Normalized residual vs. normalized iteration number for TE case at a resonant frequency ($ka = 10.173$). Computations performed using 64 bit (16–17 significant figure) word lengths and 200 unknowns.

In Figure 5.8 the convergence rate of the normalized residual is shown for the TE case at a frequency such that $ka = 10.9$. This frequency is between internal resonant frequencies of the cylinder. The associated computations were performed in single precision in Fig. 5.8 and in double precision in Fig. 5.9. Note that in this non-resonant cylinder case, little improvement in the convergence rate results from increasing the precision of the computation. Although both the EFIE and MFIE exhibit considerable variation in rate of convergence, there are no well-defined plateaus.

The above results and the fact that the conjugate gradient method stagnates if either residuals or search vectors are homogeneous solutions of the associated matrix equation leads us to conjecture that such plateaus are associated with high-Q resonances; these are in turn associated with small matrix eigenvalues and large condition numbers. We further conjecture that in structures with relatively low-Q external resonances—such as the circular cylinder—use of the CFIE effectively eliminates plateaus in the residual convergence curve. Finally, we suggest that it may not be possible to significantly improve the convergence behavior of the CGM by using the CFIE for struc-

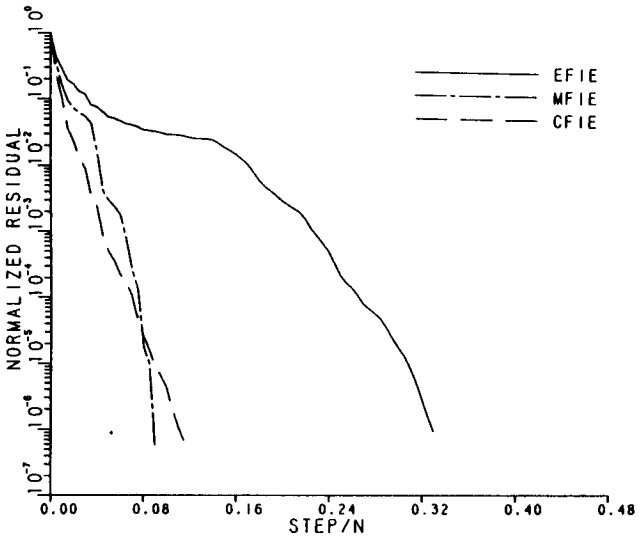

Figure 5.8 Normalized residual vs. normalized iteration number for TE incidence at a non-resonant frequency ($ka = 10.9$). Computations performed using 32 bit (7–8 significant figure) word lengths and 200 unknowns.

tures which have high-Q external resonances such as wire- or strip-like structures. This is because such structures have complex singular frequencies which are near the real frequency axis, and hence the system matrix must have at least one small eigenvalue near such frequencies.

These figures illustrate the interrelated nature of convergence rate, operator conditioning and computation accuracy. The CFIE is well-conditioned at both interior resonant and non-resonant frequencies; consequently its convergence rate is high and is not significantly affected by computational accuracy. The EFIE and MFIE are ill-conditioned near the cylinder internal resonant frequencies but are relatively well-conditioned otherwise; hence their convergence rates are affected significantly by the precision of the computation only near resonant frequencies.

Ill-conditioning can also be expected to affect the accuracy of the solutions obtained. In Figs. 5.10 and 5.11 the relative error in the TM and TE solutions, respectively, is shown for the circular cylinder very near an internal resonance ($ka = 10.73$). The quantity plotted in both figures is the difference between the computed current and the exact current normalized to twice the incident tangential compo-

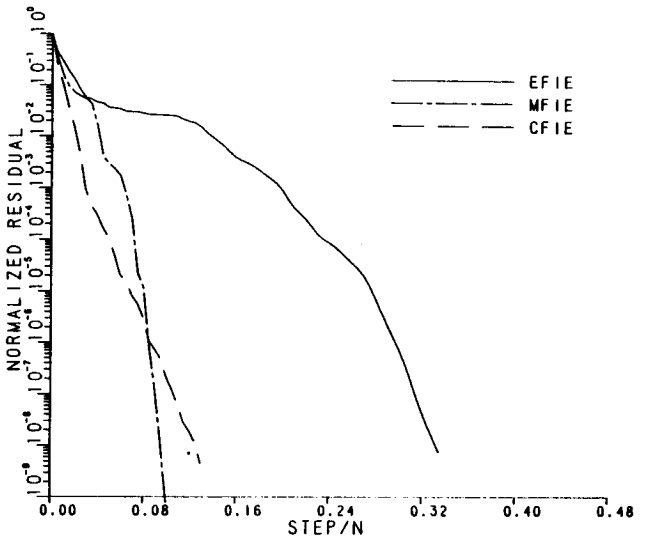

Figure 5.9 Normalized residual vs. normalized iteration number for TE incidence at a non-resonant frequency ($ka = 10.9$). Computations performed using 64 bit (16–17 significant figure) word lengths and 200 unknowns.

nent of the magnetic field ($2H_z^i$ or $2H_t^i$). The computed currents were generated by performing the CGM computations both in single and double precision and terminating the computations when the normalized residual was less than 10^{-6} for single precision and 10^{-9} for double precision. (In Fig. 5.10 the TM polarized plane wave is incident from $\phi = 0^o$, whereas in Fig. 5.11 the TE polarized plane wave is incident from $\phi = 180^o$.) It is seen that the CFIE solution is considerably more accurate in both cases than the corresponding EFIE and MFIE solutions. It is also observed that the error in the EFIE and MFIE solution oscillates at a rate corresponding to the value of m for the interior mode with spatial variation $\exp(\pm jm\phi)$ which is resonant at the solution frequency.

In Figs. 5.4–5.7 it is seen that the CFIE residual appears to exhibit exponential convergence with respect to the number of iteration steps. Furthermore, it is found that the number of steps required to achieve a normalized residual below a given level is but a slowly increasing function of the number of unknowns. This is illustrated in Figs. 5.12 and 5.13 for the TM and TE cases, respectively, by plotting the CGM convergence curves of the CFIE solution for a series of increasing fre-

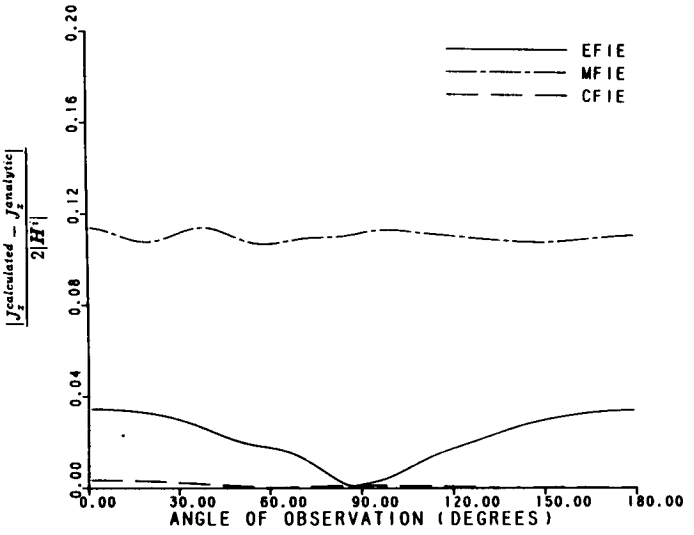

Figure 5.10 Relative error in the current distributions for TM case at a resonant frequency ($ka = 10.173$). Computations performed using double precision and 200 unknowns. Excitation field incident at 0°.

quencies as the number of unknowns is correspondingly increased. The four curves in each figure represent the normalized residual vs. number of iteration steps for circular cylinders 10, 20, 40 and 80 wavelengths in circumference using a discretization involving 100, 200, 400 and 800 unknowns, respectively. As the figures illustrate for both polarizations, not only is the convergence rate high for all the frequencies considered, but it is also remarkably insensitive to the electrical size of the scatterer.

The circular cylinder provides a good starting point for our comparisons; however, its high degree of symmetry can sometimes provide deceptive results. To address this possibility, elliptic cylinders of various aspect ratios were solved using the CFIE. Figures 5.14 and 5.15 show that though the convergence properties do not depend strongly on the shape of the body for either TM or TE incident fields, they do tend to confirm our conjecture that the increased Q of exterior resonances for thinner objects would decrease the convergence rate of the CGM.

Of significant interest are the three-dimensional formulations, for which only the EFIE and CSIE are considered here. We examine a

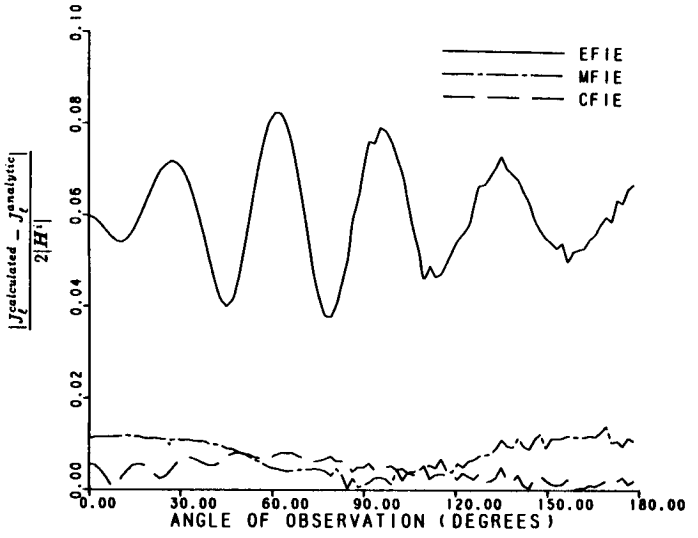

Figure 5.11 Relative error in the current distributions for TE case at a resonant frequency ($ka = 10.173$). Computations performed using double precision and 200 unknowns. Excitation field incident at 180°.

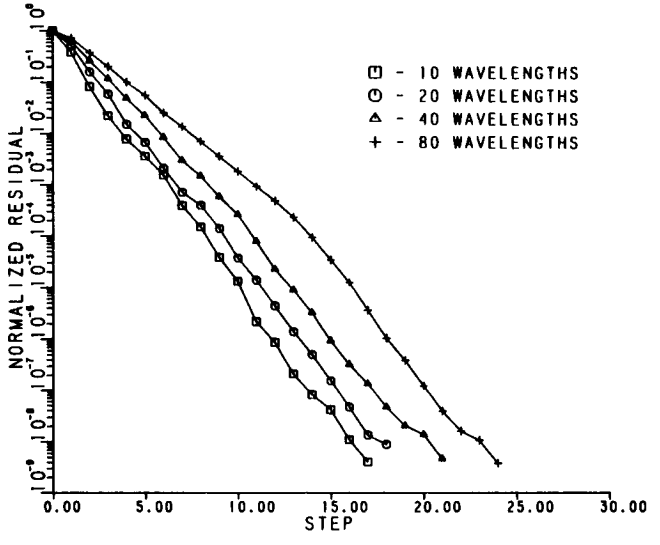

Figure 5.12 Normalized residual versus iteration number for TM case over a three octave frequency range.

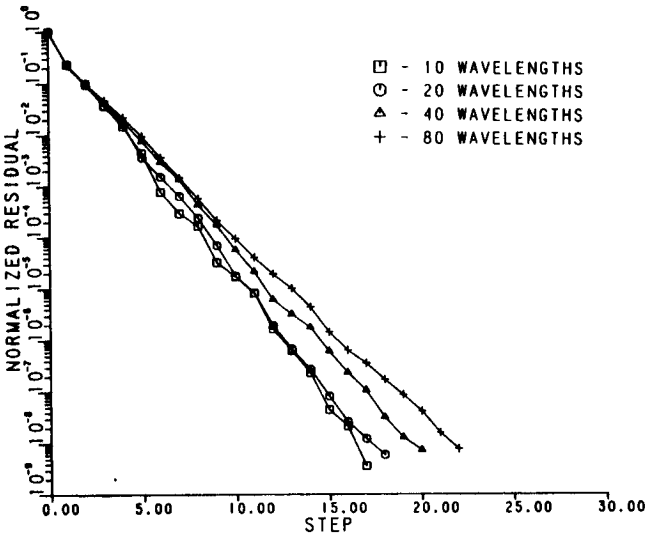

Figure 5.13 Normalized residual versus iteration number for TE case over a three octave frequency range.

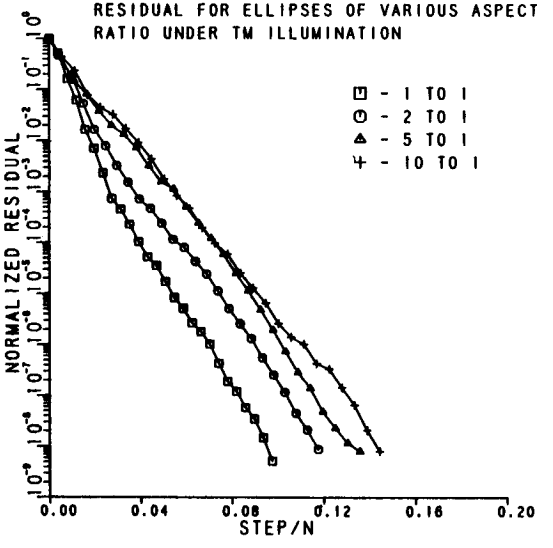

Figure 5.14 Normalized residual versus normalized iteration number for TM incidence on ellipses of various aspect ratios with $ka = 20$ where a is the semimajor axis.

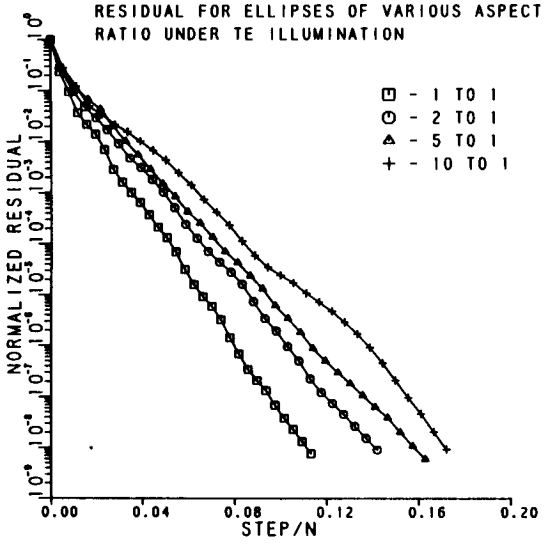

Figure 5.15 Normalized residual versus normalized iteration number for TE incidence on ellipses of various aspect ratios with $ka = 20$ where a is the semimajor axis.

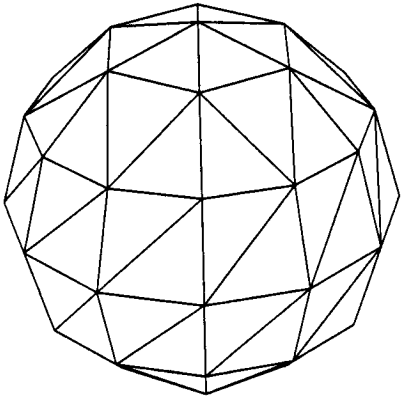

***Figure* 5.16 Triangular patch model for a sphere of diameter $\lambda/2$. Model uses 144 unknown edge currents.**

sphere and a finite circular cylinder with a diameter to length ratio of 5 to 1. The excitation in both cases consists of a uniform voltage discontinuity distributed along a delta-gap about the sphere's equator or the cylinder's circumference and centered along its length. Figures 5.16 and 5.17 show the triangular patch models used to represent the sphere at the two frequencies considered. Figures 5.18 and 5.19 show the cylinder models. Sufficient unknowns are used such that the longest edge is about $\lambda/6$ in length. Figs. 5.20 and 5.21 illustrate that the far fields of the EFIE and CSIE solutions for the discrete sphere models are in good agreement with the analytically derived results for a smooth sphere at each frequency. Figs. 5.22 and 5.23 illustrate the convergence rates of the residuals for the CGM solutions of the sphere and cylinder problems, respectively. Convergence rates are rapid for the CSIE and, as with the CFIE, the *total* number of steps to achieve a given residual error appears to be only weakly dependent on the frequency and the number of unknowns. Actually, for the cases considered, the number of steps for the EFIE—though greater than for the CFIE—also exhibits only this same weak dependence. It is not expected that this result would hold at higher frequencies, however, where the denseness of the internal resonances would strongly affect the conditioning of the EFIE. Also note that for these antenna problems, for which the spatially concentrated excitation should strongly excite more eigenfunctions of the operator than the corresponding scattering problem, rapid convergence of the CGM solution of the CFIE is still obtained.

5.5 Summary and Discussion

The electric, magnetic, and combined field integral equations are compared with respect to their influence on the convergence rate of the conjugate gradient method. Circular and elliptic cylinders under TE and TM illumination were used as test objects because the exterior resonances are of relatively low Q. Additionally, the circular cylinder solutions can be easily found analytically and compared with the numerical solutions.

To investigate three-dimensional problems the combined source integral equation is compared with the electric field integral equations with respect to convergence rate. A sphere, for which analytical results are available for comparison, and a cylinder of 5 to 1 aspect ratio were

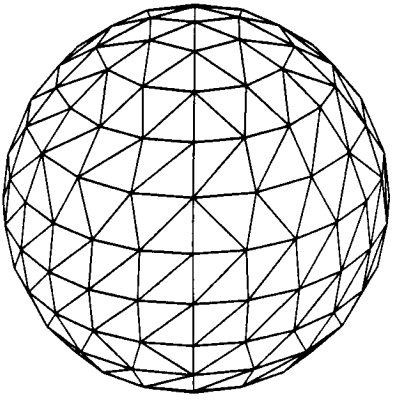

Figure 5.17 Triangular patch model for a sphere of diameter λ. Model uses 540 unknown edge currents.

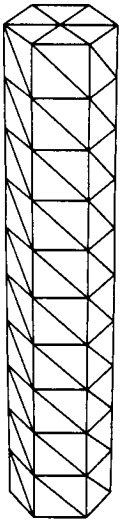

Figure 5.18 Triangular patch model for a cylinder of diameter $\lambda/4$ and length 2.5λ. Model has 198 unknown edge currents.

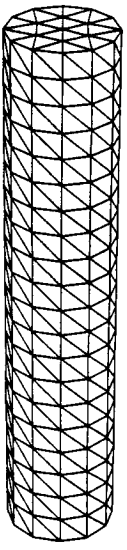

Figure 5.19 Triangular patch model for a cylinder of diameter $\lambda/2$ and length 5λ. Model has 792 unknown edge currents.

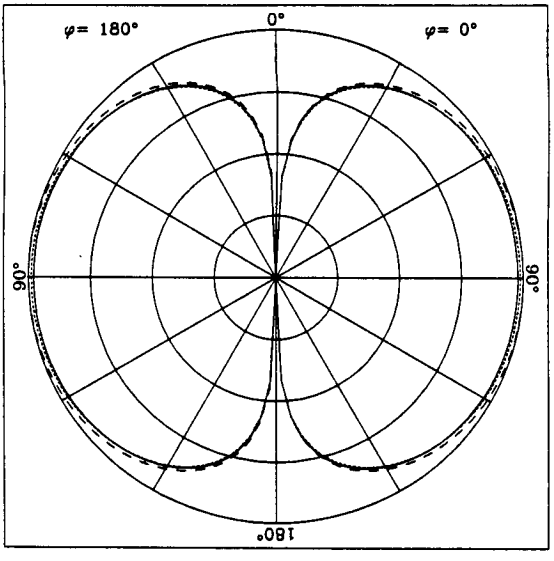

Figure 5.20 Far field pattern of sphere of $\lambda/2$ diameter excited by a uniform voltage at the equator. Patterns represent $|E_\theta|$ of the analytic (solid line), EFIE (dashed line) and CSIE (dotted line) solutions.

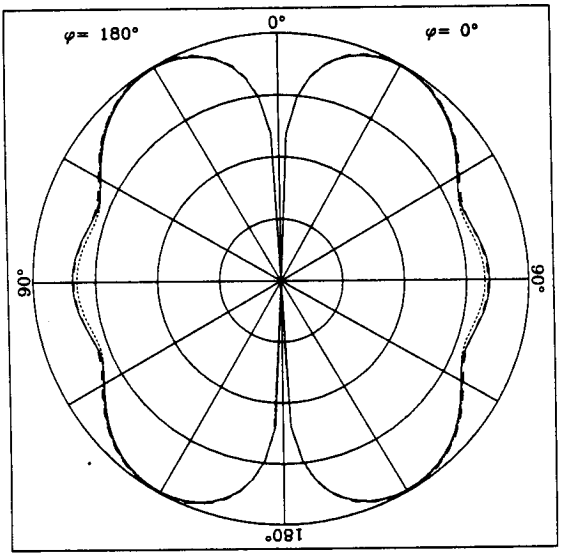

Figure 5.21 Far field pattern of sphere of λ diameter excited by a uniform voltage at the equator. Patterns represent $|E_\theta|$ of the analytic (solid line), EFIE (dashed line) and CSIE (dotted line) solutions.

used as test cases.

The most significant difficulty with the EFIE and MFIE scattering formulations at the higher frequencies—their poor conditioning at or near internal body resonances—also appears to be the principal cause of poor convergence of the CGM. It appears that both these difficulties may be overcome by using the CFIE or CSIE formulation. Under these formulations, the convergence rate of the CGM is found to be approximately exponential and, at least in the two-dimensional cases tested, only mildly dependent on the electrical size of the scatterer.

For structures which have high-Q exterior resonances (such as wire objects or cylinders of long and electrically narrow cross sections illuminated in the TE polarization), the fact that the associated integral equations must have homogeneous solutions at complex frequencies near the real frequency axis implies that the operators have small eigenvalues at nearby (real) frequencies. This in turn suggests that the operators are inherently ill-conditioned near such frequencies and that slower convergence of the CGM in the vicinity of such frequencies is to be expected.

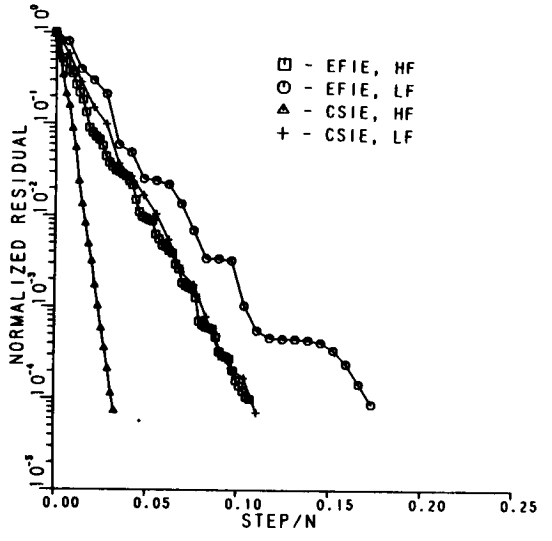

Figure 5.22 Normalized residuals of the sphere problem using the EFIE and CSIE.

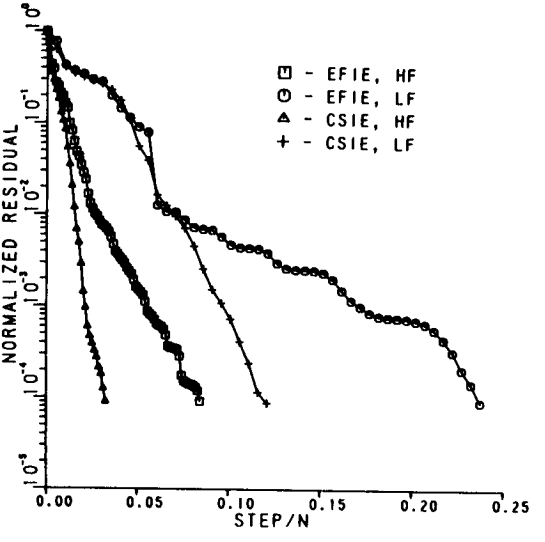

Figure 5.23 Normalized residuals of the cylinder problem using the EFIE and CSIE.

Acknowledgments

Research suppported under a contract from Texas Instruments, Incorporated, Dallas, TX.

References

[1] Peterson, A. F., and R. Mittra, "Convergence of the conjugate gradient method when applied to matrix equations representing electromagnetic scattering problems," *IEEE Trans. Antennas Propagat.*, **AP-34(12)**, 1447–1454, December 1986.

[2] Siarkiewicz, K. R., T. K. Sarkar and R. F. Stratton, "Survey of numerical methods for solution of large systems of linear equations for electromagnetic field problems," *IEEE Trans. Antennas Propagat.*, **AP-29(6)**, 847–856, August 1981.

[3] Peterson, A. F., and R. Mittra, "Method of conjugate gradients for the numerical solution of large-body electromagnetic scattering problems," *J. Opt. Soc. Am. A*, **2(6)**, 971–977, June 1985.

[4] Arvas, E., and T. K. Sarkar, "On a class of finite step iterative methods (conjugate directions) for the solution of an operator equation arising in electromagnetics," *IEEE Trans. Antennas Propagat.*, **AP-33(10)**, 1058–1066, December 1986.

[5] Sarkar, T. K., and S. M. Rao, "The application of the conjugate gradient method for the solution of electromagnetic scattering from arbitrarily oriented wire antennas," *IEEE Trans. Antennas Propagat.*, **AP-32(4)**, 398–403, April 1984.

[6] Peterson, A. F., C. F. Smith and R. Mittra, "The performance of preconditioned iterative methods when applied to electromagnetics problems," *URSI Symposium*, Blacksburg, Virginia, 1987.

[7] Kas, A., and E. L. Yip, "Preconditioned conjugate gradient methods for solving electromagnetic problems," *IEEE Trans. Antennas and Progagat.*, **AP-35(2)**, 147–152, February 1987.

[8] Mautz, J. R., and R. F. Harrington, "H-field, E-field, and combined field solutions for conducting bodies of revolution," *AEÜ*,

32(4), 157–164, April 1978.

[9] Poggio, and Miller, "Integral equation solutions of three-dimensional scattering problems," R. Mittra, editor, *Computer Techniques for Electromagnetics,* chapter 4, 173–176, Pergammon, New York, 1973.

[10] Harrington, R. F., *Time Harmonic Electromagnetic Fields,* McGraw-Hill, New York, 1961.

[11] Mautz, J. R., and R. F. Harrington, "A combined source solution for radiation and scattering from a perfectly conducting body," *IEEE Trans. Antennas Propagat.,* **AP-27(4)**, 445–454, July 1979.

[12] Hestenes, M. R., and E. Stiefel, "Methods of conjugate gradients for solving linear systems," *J. Res. Nat. Bur. Standards,* **49(6)**, 409–436, December 1952.

[13] Burden, R. L., and J. D. Faires, *Numerical Analysis,* Prindle, Weber & Schmidt, Boston, 1985.